Progress In Electromagnetics Research C, Vol. 135, 195–210, 2023

An Improved Model-Free Sliding Mode Control Algorithm of Super-Twisting for SPMSM

Xiangfei Li, Junqin Liu, Kaihui Zhao, Yang Yin, and Lihua Zou*

Abstract—An improved model-free nonsingular fast terminal sliding mode control (IMFNFTSMC) algorithm based on super-twisting extended sliding mode disturbance observer (STESMDO) is proposed to address the problems of control performance degradation and system failure of surface-mounted permanent magnet synchronous motor (SPMSM) under complex operating conditions. Firstly, the mathematical model of SPMSM under parameter ingestion is established; secondly, a novel hyperlocal model is proposed to combine with variable exponential approach law and the nonsingular fast terminal sliding mode (NFTSM) surface to design the speed-loop IMFNFTSM controller to accelerate the system convergence while reducing the sliding mode jitter. To enhance the control accuracy, the super-twisting extended sliding mode disturbance observer (STESMDO) is designed to estimate and feed-forward compensate the system disturbance. Finally, the effectiveness and superiority of the designed algorithms are demonstrated by comparing the proposed method with PI and the conventional model-free nonsingular fast terminal sliding mode control algorithm (MFNFTSMC) through simulations and RT-Lab experiments.

1. INTRODUCTION

Permanent magnet synchronous motor (PMSM) has been widely used in transportation and high-precision medical equipment because of its simple structure, small size, and high power density [1]. However, the overall motor control system is susceptible to the aging of machinery and equipment as well as harsh working environments, resulting in reduced stability [2]. Conventional proportional-integral (PI) control is prone to integral saturation, and it is difficult to effectively suppress the effects of uncertainties such as external disturbances on the control system, which cannot meet the requirements of high-precision control performance [3]. Sliding mode control (SMC) is widely used because of its good transient performance and robustness [4]. However, the conventional SMC method suffers from dithering, which may cause large system errors [5].

In response to these issues, many scholars have conducted experimental discussions on reducing sliding mode chattering. A nonsingular terminal sliding mode control strategy is proposed in [6], which enables the terminal sliding mode singularity problem to be solved and improves the response speed of the system, but the tracking performance of the system decreases. Compared with [6, 7], an improved nonsingular terminal sliding mode and a perturbation observer are combined to design a controller for speed, which solves the singularity problems while achieving accurate tracking. In [8], a special and simple super-twisting sliding mode control algorithm in higher-order sliding mode control is used, which is able to suppress the jitter of the system substantially. Ref. [9] analyzes the specific implementation process of the super-twisting second-order sliding mode and how to construct the super-twisting second-order sliding mode observer. The current tracking control method based on super-twisting second-order sliding mode control is proposed to be applied to the control of active power filters in [10]. Ref. [11]

Received 15 June 2023, Accepted 19 July 2023, Scheduled 4 August 2023
* Corresponding author: Lihua Zou (zoulihua0518@163.com).
The authors are with the College of Electrical and Information Engineering, Hunan University of Technology, Zhuzhou 412007, China.

compares the jitter of the conventional second-order super-twisting control law with conventional sliding mode control law, and concludes that them can suppress the jitter. In [12], a super-twisting second-order sliding mode was used for the control of an autonomous underwater glider, and its control performance was compared with the conventional sliding mode control. It is known from [8–12] that the combination of sliding mode control can enhance the immunity of passive control, while the super-twisting second-order sliding mode can further suppress the jitter. Therefore, a passive super-twisting second-order sliding mode control strategy for unified power quality conditioner based on modular multilevel converter (MMC-UPQC) is proposed in [13], which combines the passive control law and super-twisting second-order sliding mode control law to improve the current inner loop of the system and enhance the fast response capability, compensation quality, and interference immunity of the system. In [14], a novel dilated state observer based on generalized super-twisting theory is designed to estimate the unknown set of total perturbations and compensate the estimated values to the speed controller of PMSM to effectively improve the robustness of system under load torque and inertia variations.

The above literature results show that the super-twisting second-order sliding mode control algorithm effectively suppresses jitter and improves the dynamic and static quality, while retaining the advantages of traditional sliding mode control. For the existence of limited jitter suppression, anti-interference ability and other problems, this paper proposes an improved model-free nonsingular fast terminal sliding mode control (IMFNFTSMC) algorithm for SPMSM based on a new super-twisting extended sliding mode disturbance observer (STESMDO). Firstly, the novel hyperlocal model is proposed to combine the second-order super-twisting with nonsingular fast terminal sliding mode (NFTSM) surface designing a speed loop controller to improve the speed tracking performance. STESMDO is designed to estimate system disturbance and provide feedback to the controller as a means of implementing SPMSM fault-tolerant control under complex operating conditions. Finally, the effectiveness of the proposed algorithm is verified by simulation and RT-Lab experiments.

2. MATHEMATICAL MODEL OF SPMSM

The SPMSM operates in the ideal state with the mathematical formula can be expressed as [15]:

$$\begin{cases} T_e = \dfrac{3}{2} n_p \psi_f i_q \\ \dfrac{d\omega_e}{dt} = \dfrac{n_p}{J}\left(T_e - T_L - B\omega_m\right) \\ u_d = R_s i_d + L_d \dfrac{di_d}{dt} - \omega_e L_q i_q \\ u_q = R_s i_q + L_q \dfrac{di_q}{dt} + \omega_e \left(L_d i_d + \psi_f\right) \end{cases} \tag{1}$$

where i_d is the stator d-axis current; i_q is the stator q-axis current; u_d is the stator d-axis voltage; u_q is the stator q-axis voltage; L_d is the stator winding d-axis inductance; L_q is the stator winding q-axis inductance; ω_e is the electrical angular velocity; T_e is the PMSM output electromagnetic torque; T_L is the load torque; J is the rotational inertia; B is the damping factor; ω_m is the mechanical angular velocity of the motor; ψ_f is the permanent magnet flux; R_s is the stator resistance; n_p is the number of pole pairs.

Considering the impact of SPMSM operation on system stability under complex conditions, the mathematical model of SPMSM can be further obtained as [15]:

$$\begin{cases} T_e = \dfrac{3}{2} n_p \psi_f i_q + \Delta T_e \\ \dfrac{d\omega_e}{dt} = \dfrac{n_p}{J}\left(T_e - T_L - B\omega_m\right) + \Delta P_n \\ u_d = R_s i_d + L_d \dfrac{di_d}{dt} - \omega_e L_q i_q + \Delta u_d \\ u_q = R_s i_q + L_q \dfrac{di_q}{dt} + \omega_e (L_d i_d + \psi_f) + \Delta u_q \end{cases} \tag{2}$$

where Δu_d is the d-axis voltage disturbance under complex conditions; Δu_q is the q-axis voltage disturbance under complex conditions; ΔP_n is the disturbance caused by the change of J and B; ΔT_e is the output electromagnetic torque disturbance under complex conditions.

The combination of (1) and (2) can be obtained:

$$\frac{d\omega_e}{dt} = 3n_p^2\psi_f/2J \cdot i_q - B/J \cdot \omega_e + n_p\left(\Delta T_e - T_L + \Delta T_L\right)/J + \Delta P_n \tag{3}$$

3. DESIGN OF IMFNFTSM CONTROLLER

To ensure that SPMSM still has high-performance, this section first establishes a new hyperlocal model of SPMSM speed loop, designs a second-order superhelix control law combined with NFTSM, and proposes an IMFNFTSM control strategy; under complex operating conditions, the algorithm can both effectively reduce jitter and accelerate system convergence.

3.1. Build of a New HYPERLOCAL Model for SPMSM

The first-order nonlinear hyperlocal model can be expressed as [16]:

$$\begin{cases} y = x \\ \dot{x} = \lambda_1 u + g(x) \end{cases} \tag{4}$$

where $x \in \mathrm{K}$ is the state variable of the system; y is the output of the system control; u is the input of the system control; $\lambda_1 \in \mathrm{K}$ is the gain constant to be designed.

From Eq. (4), $g(x)$ can be expressed as:

$$g(x) = \lambda_2 x + F \tag{5}$$

where λ_2 is the state gain of the system to be designed; F is the unknown part.

Combining Eq. (4) and Eq. (5), the new hyperlocal model of the rotational speed loop can be built as [16]:

$$\begin{cases} y = x \\ \dot{x} = \lambda_1 u + \lambda_2 x + F \end{cases} \tag{6}$$

To ensure the high control performance under the PMSM parameter uptake and time-varying perturbation, the new hyperlocal model of the speed loop can be designed as:

$$\begin{cases} \dfrac{d\omega_e}{dt} = \lambda_1 i_q + \lambda_2 \omega_e + F \\ \dfrac{dF}{dt} = \Lambda(t) \end{cases} \tag{7}$$

where $\lambda_1 = 3n_p^2\psi_f/2J$; $\lambda_2 = -B/J$.

3.2. Design of Speed IMFNFTSM Controller for SPMSM

From Eq. (3) and Eq. (7), the control law of i_q^* for the speed controller can be designed as:

$$i_q^* = \frac{\dot{\omega}_e^* - \lambda_2\omega_e - F + u_c}{\lambda_1} \tag{8}$$

Define the e:

$$e = \omega_e^* - \omega_e \tag{9}$$

Combine Eq. (8) and Eq. (9):

$$\dot{\omega}_e^* - \dot{\omega}_e = -u_c \tag{10}$$

The design equation of state is $\dot{e}_1 = e_2$ and $\dot{e}_2 = \dot{e}$. For Eq. (10), the NFTSM surface is chosen as [17]:

$$s = e_1 + \alpha e_1^{\alpha_1} + \beta e_2^{\beta_1} \tag{11}$$

where $\alpha > 0$; $\beta > 0$; $\alpha_1 = g/h$; $\beta_1 = p/q$; $1 < \beta_1 < 2$; $\alpha_1 > \beta_1$.

The derivative of Eq. (11) is obtained:

$$\dot{s} = \dot{e}_1 + \alpha\alpha_1 e_1^{\alpha_1 - 1} e_2 + \beta\beta_1 e_2^{\beta_1 - 1}\dot{e}_2 \tag{12}$$

To improve the shortcomings of the traditional exponential convergence law because of the large parameter gain resulting in large jitter, this paper proposes a variable exponential convergence law, which takes the following form [18]:

$$\begin{cases} \dot{s} = -l_1 |x|^{\frac{1}{2}} \operatorname{sgn}(s) - l_2 f(s) \\ f(s) = \begin{cases} s & |s| \geq \mu \\ \operatorname{sgn}(s) & |s| < \mu \end{cases} \end{cases} \tag{13}$$

where $l_1 > 0$; $l_2 > 0$; l_1, l_2 are the parameters to be designed; $|x|$ is the system state variable; $f(s)$ is the designed nonlinear function; μ is a tiny positive real number. By introducing the system state variable x in the isokinetic term, it can make the value of $|x|$ larger when the state variable is far from the sliding mode surface, thus speeding up the system response and playing the effect of accelerating the convergence to the sliding mode surface; approaching the sliding mode surface, introducing the nonlinear function $f(s)$ in the improved exponential term can make the effect of effectively limiting the amplitude and reducing the amplitude of the sliding mode quantity at $|s| > q$; while $|s| \leq q$, adding the improved power term to ensure the finite-time convergence of the state variables and improve the response speed.

Theorem 1: From Eq. (10)–(13), the u_c for IMFNFTSMC can be designed as Eq. (14), and e will converge.

$$u_c = \frac{1}{\beta\beta_1} e_2^{2-\beta_1} \cdot \left(1 + \alpha\alpha_1 e_1^{\alpha_1 - 1}\right) + l_1 |x|^{\frac{1}{2}} \operatorname{sgn}(s) + l_2 f(s) \tag{14}$$

Proof 1: Taking the following positive definite Lyapunov function V_1:

$$V_1 = \frac{1}{2} s^2 \tag{15}$$

Taking the derivative of Eq. (15) and substituting Eq. (11), Eq. (16) can be expressed as:

$$\begin{aligned} V_1 = s\dot{s} &= s \cdot \left(-l_1 |x|^{\frac{1}{2}} \operatorname{sgn}(s) - l_2 f(s)\right) \\ &= -l_1 |x|^{\frac{1}{2}} s \cdot \operatorname{sgn}(s) - l_2 \cdot s \cdot f(s) \end{aligned} \tag{16}$$

While $|s| \geq \mu$:

$$\begin{aligned} \dot{V}_1 &= -l_1 |x|^{\frac{1}{2}} s \cdot \operatorname{sgn}(s) - l_2 \cdot s \cdot f(s) \\ &\leq -l_1 |x|^{\frac{1}{2}} s - l_2 \cdot s^2 \\ &\leq -s \left(l_1 |x|^{\frac{1}{2}} + l_2 s\right) \\ &\leq 0 \end{aligned} \tag{17}$$

While $|s| < \mu$:

$$\begin{aligned} \dot{V}_1 &= -l_1 |x|^{\frac{1}{2}} s \cdot \operatorname{sgn}(s) - l_2 \cdot s \cdot f(s) \\ &\leq -l_1 |x|^{\frac{1}{2}} s - l_2 \cdot s \\ &\leq -s \left(l_1 |x|^{\frac{1}{2}} + l_2\right) \\ &\leq 0 \end{aligned} \tag{18}$$

From Eq. (17) and Eq. (18), $\dot{V}_1 \leq 0$ is constant, and the designed control law satisfies Lyapunov stability. From Eq. (11) to (14), the overall control law of i_q^* can be obtained as:

$$\begin{aligned} i_q^* &= \frac{\dot{\omega}_e^* - \lambda_2 \omega_e - F + u_{\mathrm{C}}}{\lambda_1} \\ &= \frac{1}{\lambda_1} \left[\dot{\omega}_e^* + \frac{1}{\beta\beta_1} e_2^{2-\beta_1} \cdot \left(1 + \alpha\alpha_1 e_1^{\alpha_1 - 1}\right) + l_1 |x|^{\frac{1}{2}} \operatorname{sgn}(s) + l_2 f(s) - \lambda_2 \omega_2 - F\right] \end{aligned} \tag{19}$$

3.3. Design of STESMDO for IMFNFTSM Controller

The STESMDO improves the severe system jitter caused by conventional sliding mode disturbance observer (SMO), because of its high gains. Define the variables as follows:

$$s_1 = \hat{\omega}_e - \omega_e \tag{20}$$

Equation (7) is redefined as [19]:

$$\begin{cases} \dfrac{d\hat{\omega}_e}{dt} = \lambda_1 i_q + \lambda_2 \hat{\omega}_e + \hat{F} + u_{STESMDO} \\ \dfrac{d\tilde{F}}{dt} = H \cdot u_{STESMDO} \end{cases} \tag{21}$$

where $\hat{\omega}_e$ is the tracking speed of STESMDO; $\hat{F}$ is the estimated value of the system disturbance; $H > 0$; $\tilde{F} = \hat{F} - F$.

From Eq. (7) and Eq. (21):

$$\begin{cases} \dot{s}_1 = \lambda_2 s_1 + \tilde{F} + u_{STESMDO} \\ \dfrac{d\tilde{F}}{dt} = H \cdot u_{STESMDO} - \Lambda(t) \end{cases} \tag{22}$$

where $\Lambda(t) = dF/dt$.

Design second-order super-twisting control laws [20]:

$$\begin{cases} \dot{s}_1 = -k_1 \left|s_1\right|^{\frac{1}{2}} \operatorname{sgn}(s_1) + g + \tilde{F} \\ \dot{g} = -k_2 \operatorname{sgn}(s_1) \end{cases} \tag{23}$$

From Eqs. (21)–(23), the control law of STESMDO can be expressed as:

$$u_{STESMDO} = -\lambda_2 s_1 - k_1 \left|s_1\right|^{\frac{1}{2}} \operatorname{sgn}(s_1) - \int k_2 \operatorname{sgn}(s_1) \tag{24}$$

Theorem 2: According to the quadratic and Lyapunov stability theorems [15], it is known that the super-twisting (ST) control law will converge the system error in finite time when Eq. (25) is satisfied.

$$\begin{cases} k_1 > \dfrac{\left(4k_2 + k_1^2\right)\delta_1}{\left(2k_2 + k_1^2\right)} \\ k_2 > \dfrac{16k_2\delta_1 + k_1\delta_1^2}{8k_1} \end{cases} \tag{25}$$

Proof 2: Choosing a Lyapunov function $V_1(x)$:

$$\begin{aligned} V_1(x) &= 2k_2 \left|s\right| + \frac{1}{2}g^2 + \frac{1}{2}\left(k_1 \left|s\right|^{\frac{1}{2}} \operatorname{sgn}(s) - \mathbf{g}\right)^2 \\ &= \frac{1}{2}\left(4k_2 + k_1^2\right)\left|s\right| + \mathbf{g}^2 - k_1 \mathbf{g} \left|s\right|^{\frac{1}{2}} \operatorname{sgn}(s) \\ &= \frac{1}{2}\begin{bmatrix} \left|s\right|^{\frac{1}{2}} \operatorname{sgn}(s) & \mathbf{g} \end{bmatrix} \begin{bmatrix} 4k_2 + k_1^2 & -k_1 \\ -k_1 & 2 \end{bmatrix} \begin{bmatrix} \left|s\right|^{\frac{1}{2}} \operatorname{sgn}(s) \\ \mathbf{g} \end{bmatrix} \end{aligned} \tag{26}$$

Equation (26) can be reduced as:

$$V_1 = \zeta^T \mathbf{P} \zeta \tag{27}$$

where $\zeta^T = \begin{bmatrix} \left|s\right|^{\frac{1}{2}} \operatorname{sgn}(s) & \mathbf{g} \end{bmatrix}$; $P = \frac{1}{2}\begin{pmatrix} 4k_2 + k_1^2 & -k_1 \\ -k_1 & 2 \end{pmatrix}$; $\mathbf{P}$ is a positive definite and continuous matrix, because $k_1 > 0$ and $k_2 > 0$.

The derivative of ζ is obtained as:

$$\begin{aligned}\dot{\zeta} &= \begin{bmatrix} \frac{1}{2}\frac{1}{|s|^{\frac{1}{2}}}\cdot\dot{s} \\ \dot{\mathbf{g}} \end{bmatrix} = \frac{1}{|s|^{\frac{1}{2}}}\begin{bmatrix} -\frac{1}{2}k_1|s|^{\frac{1}{2}}\operatorname{sgn}(s)+\frac{1}{2}\mathbf{g}+\frac{1}{2}\tilde{F} \\ -k_2|s|^{\frac{1}{2}}\operatorname{sgn}(s) \end{bmatrix} \\ &= \frac{1}{|s|^{\frac{1}{2}}}\left[\begin{bmatrix} -\frac{1}{2}k_1 & \frac{1}{2} \\ -k_2 & 0 \end{bmatrix}\zeta+\begin{bmatrix} \frac{F}{2} \\ 0 \end{bmatrix}\right] = \frac{1}{|s|^{\frac{1}{2}}}(\mathbf{A}\zeta+\eta)\end{aligned} \tag{28}$$

where $\mathbf{A}=\begin{bmatrix} -\frac{1}{2}k_1 & \frac{1}{2} \\ -k_2 & 0 \end{bmatrix}$; $\eta^T=\begin{bmatrix} \frac{\tilde{F}}{2} & 0 \end{bmatrix}$.

The derivative of $V_1(x)$ is obtained as:

$$\begin{aligned}\dot{V} &= \dot{\zeta}^T\mathbf{P}\zeta+\zeta^T\mathbf{P}\dot{\zeta} \\ &= \frac{1}{|s|^{\frac{1}{2}}}\left[\zeta^T\mathbf{A}^T+\eta^T\right]\mathbf{P}\zeta+\frac{1}{|s|^{\frac{1}{2}}}\zeta^T\mathbf{P}\left[\mathbf{A}\zeta+\eta\right] \\ &= \frac{1}{|s|^{\frac{1}{2}}}\left[\zeta^T\mathbf{A}^T\mathbf{P}\zeta+\eta^T\mathbf{P}\zeta\right]+\frac{1}{|s|^{\frac{1}{2}}}\left[\zeta^T\mathbf{P}\mathbf{A}\zeta+\zeta^T\mathbf{P}\eta\right] \\ &= -\frac{1}{|s|^{\frac{1}{2}}}\zeta^T\mathbf{Q}\zeta+\frac{\rho}{|s|^{\frac{1}{2}}}\mathbf{q}_1^T\zeta \\ &\le -\frac{1}{|s|^{\frac{1}{2}}}\zeta^T\mathbf{Q}\zeta+\delta_1\mathbf{q}_1^T\zeta\end{aligned} \tag{29}$$

where $\mathbf{Q}=\frac{k_1}{2}\begin{bmatrix} 2k_2+k_1^2 & -k_1 \\ -k_1 & 1 \end{bmatrix}$; $\mathbf{q}_1^T=\begin{bmatrix} \left(2k_2+\frac{k_1^2}{2}\right) & -\frac{k_1}{2} \end{bmatrix}$; $\tilde{F}\le\delta_1|s|^{\frac{1}{2}}$.

The range of values of $\delta_1\mathbf{q}_1^T\zeta$ in Eq. (26) is obtained as:

$$\begin{aligned}\delta_1\mathbf{q}_1^T\zeta &= \delta_1\begin{bmatrix} \left(2k_2+\frac{k_1^2}{2}\right) & -\frac{k_1}{2} \end{bmatrix}\begin{bmatrix} |s|^{\frac{1}{2}}\operatorname{sgn}(s) \\ \mathbf{g} \end{bmatrix} \\ &= \frac{\delta_1}{|s|^{\frac{1}{2}}}\left[\left(2k_2+\frac{k_1^2}{2}\right)|s|^{\frac{1}{2}}|s|^{\frac{1}{2}}\operatorname{sgn}(s)-\frac{k_1}{4}\mathbf{g}|s|^{\frac{1}{2}}-\frac{k_1}{4}\mathbf{g}|s|^{\frac{1}{2}}\right] \\ &= \frac{1}{|s|^{\frac{1}{2}}}\begin{bmatrix} |s|^{\frac{1}{2}}sgn(s) & \mathbf{g} \end{bmatrix}\frac{k_1}{2}\begin{bmatrix} \left(4\frac{k_2}{k_1}+k_1\right)\delta_1 & -\frac{1}{2}\delta_1 \\ -\frac{1}{2}\delta_1 & 0 \end{bmatrix}\operatorname{sgn}(s)\begin{bmatrix} |s|^{\frac{1}{2}}\operatorname{sgn}(s) \\ \mathbf{g} \end{bmatrix} \\ &\le \frac{1}{|s|^{\frac{1}{2}}}\begin{bmatrix} |s|^{\frac{1}{2}}\operatorname{sgn}(s) & \mathbf{g} \end{bmatrix}\frac{k_1}{2}\begin{bmatrix} \left(4\frac{k_2}{k_1}+k_1\right)\delta_1 & -\frac{1}{2}\delta_1 \\ -\frac{1}{2}\delta_1 & 0 \end{bmatrix}\begin{bmatrix} |s|^{\frac{1}{2}}\operatorname{sgn}(s) \\ \mathbf{g} \end{bmatrix} = \frac{1}{|s|^{\frac{1}{2}}}\zeta^T\mathbf{M}\zeta\end{aligned} \tag{30}$$

where $\mathbf{M}=\frac{k_1}{2}\begin{bmatrix} \left(4\frac{k_2}{k_1}+k_1\right)\delta_1 & -\frac{1}{2}\delta_1 \\ -\frac{1}{2}\delta_1 & 0 \end{bmatrix}$.

From Eq. (26) and Eq. (27):

$$\begin{aligned}
\dot{V} &\leq -\frac{1}{|s|^{\frac{1}{2}}}\zeta^T\mathbf{Q}\zeta + \delta_1 q_1^T\zeta \\
&\leq -\frac{1}{|s|^{\frac{1}{2}}}\zeta^T\mathbf{Q}\zeta + \frac{1}{|s|^{\frac{1}{2}}}\zeta^T M\zeta \\
&= -\frac{1}{|s|^{\frac{1}{2}}}\zeta^T\left[\mathbf{Q}-\mathbf{M}\right]\zeta \\
&= -\frac{1}{|s|^{\frac{1}{2}}}\zeta^T\left[\frac{k_1}{2}\begin{pmatrix} 2k_2+k_1^2-\left(\dfrac{4k_2}{k_1}+k_1\right)\delta_1 & -k_1+\dfrac{1}{2}\delta_1 \\ -k_1+\dfrac{1}{2}\delta_1 & 1 \end{pmatrix}\right]\zeta\zeta \\
&= -\frac{1}{|s|^{\frac{1}{2}}}\zeta^T\left[\tilde{\mathbf{Q}}\right]\zeta
\end{aligned} \tag{31}$$

where $\tilde{\mathbf{Q}} = \frac{k_1}{2}\begin{bmatrix} 2k_2+k_1^2-\left(\frac{4k_2}{k_1}+k_1\right)\delta_1 & -k_1+\frac{1}{2}\delta_1 \\ -k_1+\frac{1}{2}\delta_1 & 1 \end{bmatrix}$.

From the properties of Schur complement:

$$\begin{cases} 2k_2+k_1^2-\left(\dfrac{4k_2}{k_1}+k_1\right)\delta_1 > 0 \\ 1-\left(-k_1+\dfrac{1}{2}\delta_1\right)^2\left[2k_2+k_1^2-\left(\dfrac{4k_2}{k_1}+k_1\right)\delta_1\right]^{-1} > 0 \end{cases} \tag{32}$$

Eq. (32) is simplified as:

$$\begin{cases} k_1 > \dfrac{\left(4k_2+k_1^2\right)\delta_1}{\left(2k_2+k_1^2\right)} \\ k_2 > \dfrac{16k_2\delta_1+k_1\delta_1^2}{8k_1} \end{cases} \tag{33}$$

If the range of values of k_1 and k_2 satisfies the Eq. (34), $\tilde{Q}$ is positive definite:

$$\begin{aligned}
\dot{V} &\leq -\frac{1}{|s|^{\frac{1}{2}}}\zeta^T\tilde{\mathbf{Q}}\zeta \\
&\leq -\frac{1}{|s|^{\frac{1}{2}}}\lambda_{\min}\left\{\tilde{\mathbf{Q}}\right\}\|\zeta\|_2^2 \leq -\gamma V^{\frac{1}{2}} \leq 0
\end{aligned} \tag{34}$$

From Eq. (34), the whole system is stable. Substituting Eq. (24) into Eq. (22), the expression of F can be expressed as:

$$\hat{F} = H\int\left(-\lambda_2 s_1 - k_1|s_1|^{\frac{1}{2}}\mathrm{sgn}(s_1) - k_2\mathrm{sgn}(s_1)\right)dt \tag{35}$$

Substituting Eq. (35) into Eq. (19), the total control law i_q^* can be expressed as:

$$i_q^* = \frac{\dot{\omega}_e^* - \lambda_2\omega_e - F + u_{\mathrm{C}}}{\lambda_1} = \frac{1}{\lambda_1}\left[\dot{\omega}_e^* + \frac{1}{\beta\beta_1}e_2^{2-\beta_1}\cdot\left(1+\alpha\alpha_1 e_1^{\alpha_1-1}\right) + l_1|x|^{\frac{1}{2}}\mathrm{sgn}(s)l_2 f(s) - \lambda_2\omega_e\hat{F}\right] \tag{36}$$

To effectively reduce the jitter, the saturation function $\Re(s)$ is used to replace the *sign*:

$$\Re(s) = \frac{2}{1+\exp^{-\tau s}} \tag{37}$$

where $\tau > 0$. Fig. 1 is the block diagram of IMFNFTSMC based on STESMDO. Fig. 2 is the block diagram of STESMDO.

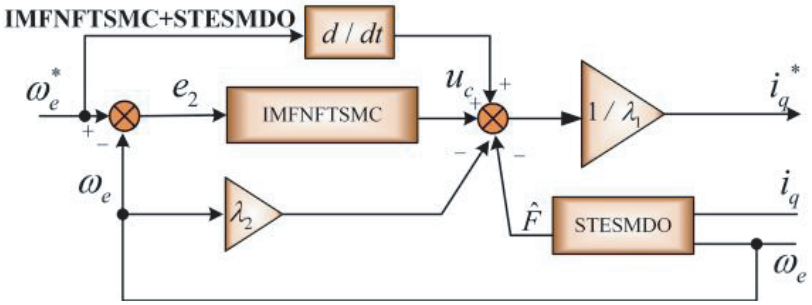

Figure 1. The block diagram of IMFNFTSMC based on STESMDO.

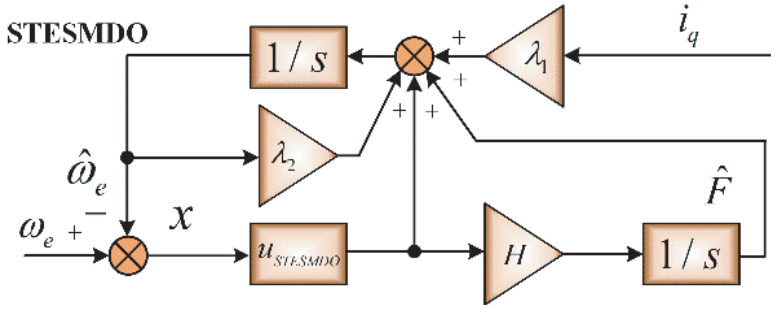

Figure 2. The block diagram of STESMDO.

4. ANALYSIS OF EXPERIMENTAL RESULTS

To verify the effectiveness of the algorithm, the STESMDO-based IMFNFTSMC algorithm proposed in the paper is built in MATLAB/Simulink platform, and compared with PI and MFNFTSMC algorithms. SPMSM uses $i_d = 0$. Table 1 is the nominal parameter of SPMSM. Fig. 3 is the control system of SPMSM.

Table 1. The motor parameters.

Motor parameters	Units	Values
Permanent magnet flux/ψ_f	Wb	0.171
d axis inductance/L_d	H	0.00334
q axis inductance/L_q	H	0.00334
stator phase resistance/R_s	Ω	1.9
pole number/n_p	Pairs	4
rotational inertia/J	$\mathrm{kg \cdot m^2}$	0.001469
damping factor/B	$\mathrm{N \cdot m \cdot s/rad}$	0.001

Remark1: In MFNTSMC algorithm, the conventional convergence law is chosen as $\dot{s} = -k_3 sgn(s) - k_4 s$*, and the conventional SMO is chosen for MFNTSMC.* λ_1 *and* λ_2 *in the system are rectified by* $\lambda_1 = 3n_p^2\psi_f/2J$ *and* $\lambda_2 = -B/J$*; the exponential parameters of g, h, p and q as state variables in the NFTSM are all positively odd,* $p/q = 5/3$*,* $g/h = 7/5$ *and* $1 < p/q < 2$*.* α *and* β *are generally chosen as the gains of the state variables, which affect the quality of the sliding modes to some extent. Therefore, based on the determination of* $\alpha > 0$ *and* $\beta > 0$*, the approximate parameters are first selected to ensure that the sliding mold surface can converge asymptotically in finite time,* $s = 0$*, and then fine-tuned.* l_1*,* l_2*,* k_3*, and* k_4 *belong to the convergence law parameters, and the method of convergence law is to*

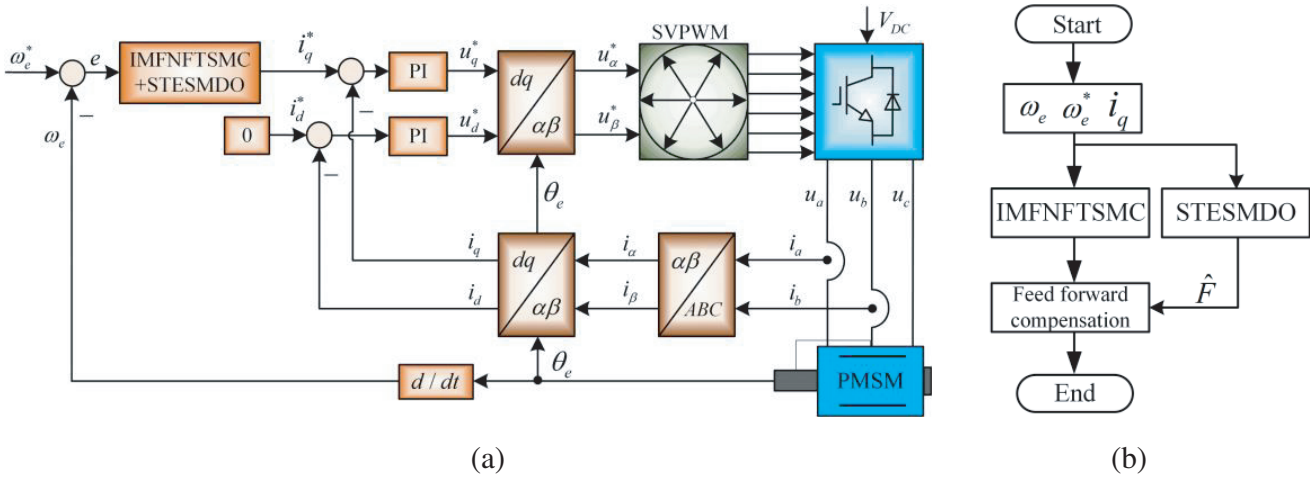

Figure 3. (a) The control system of SPMSM. (b) The flow chart of IMFNFTSMC.

improve the dynamic quality of the convergence motion of the sliding mode variable structure. l_1, l_2, k_3, *and* k_4 *mainly affect the convergence speed of the sliding mode surface, can be guaranteed under the premise of convergence of the sliding mode surface that can be converged; compare the rotational speeds in the 1000 r/min and 2000 r/min as well as the parameters of the speed of the ingestion of jitter vibration and static differentials, and the parameters of the convergence law of the fine-tuning;* σ *is used to optimize the jitter problem of the sliding mode motion, which belongs to the local optimization, and can be adjusted accordingly by observing the rotational speed jitter of the motor during steady state operation.*

4.1. Analysis of Simulation Results

Table 2 shows the parameter perturbations and external time-varying disturbances for SPMSM. IMFNFTSMC is compared with PI and MFNFTSMC to examine the anti-disturbance performance.

Table 2. The experimental condition.

Time/s	Perturbations	Range of Perturbations
0.1	R_s/Ω	1.9→2.7
0.5	ψ_f/Wb	0.171→0.11
0.6	L_s/H	0.00334→0.00467
0.7	B	0.001→0.004
0.8	J	0.001469→0.005
0.9	$T_L/\mathrm{N}\cdot\mathrm{m}$	$5\rightarrow 5+\sin 500t$
1.0	$T_L/\mathrm{N}\cdot\mathrm{m}$	$5+\sin 500t\rightarrow 5$
1.1	$T_L/\mathrm{N}\cdot\mathrm{m}$	5→10

Figure 4 is the simulations of the three algorithms. From Fig. 4(a), the PI takes a long time to reach the specified speed throughout the speed regulation condition, and there is a significant overshoot. When parameters are ingested, time-varying disturbances occurred in the PMSM, leading to large fluctuations in PI.

Compared with PI, the MFNFTSMC algorithm improves the robustness of the controller to a certain extent, but it still cannot meet the requirements of high-precision control. The IMFNFTSMC algorithm not only enables the system to reach the specified speed quickly, but also further improves

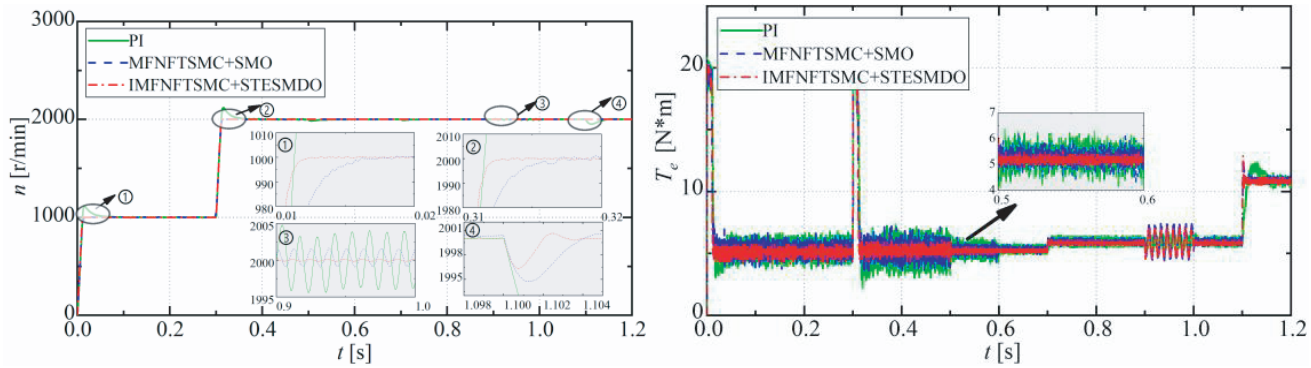

Figure 4. Simulation comparison results of PI/MFNFTSMC/IMFNFTSMC. (a) Simulation comparison of speed. (b) Simulation comparison of torque.

the robustness and control accuracy of the system, and reduces the impact of parameter ingestion and external time-varying disturbances on the speed. From Fig. 4(b), there is transient overshoot and large pulsation in the torque of PI and MFNFTSMC. In contrast, the IMFNFTSMC controlled torque pulsation can quickly track the torque reference value with less pulsation. When time-varying perturbation is added at the 0.9 s, the IMFNFTSMC fluctuates less and converges faster than the remaining two algorithms.

From Fig. 5, the *d*-*q* axis current pulsation of IMFNFTSMC is much smaller than PI and MFNFTSMC, and the current response is the fastest. In addition, the steady-state values of *q*-axis currents controlled by PI and MFNFTSMC have large steady-state error compared with IMFNFTSMC, because of the effect of motor parameter ingestion.

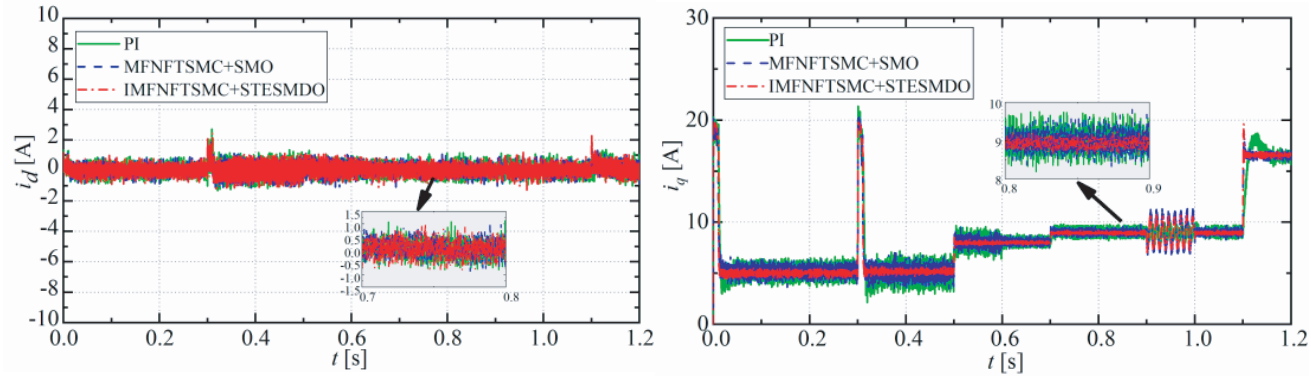

Figure 5. Simulation comparison results of PI/MFNFTSMC/IMFNFTSMC. (a) Simulation comparison of *d*-axis current. (b) Simulation comparison of *q*-axis current.

Figure 6 shows the comparisons of SMO and STESMDO. From Fig. 6(a), it can be seen that there is a small speed-tracking error in STESMDO. During the transient process of motor parameter ingestion and time-varying disturbance, the speed-tracking error of SMO is large, and the overall tracking effect is poor. From Fig. 6(b), the system perturbation estimated by STESMDO is smoother, and the jitter is smaller. The control accuracy of the controller depends, to some extent, on the accurate estimation of the disturbance amount by the disturbance observer, so the system control performance is optimal in the IMFNFTSMC algorithm.

The A-phase current waveforms of the three algorithms and their corresponding harmonic distortion

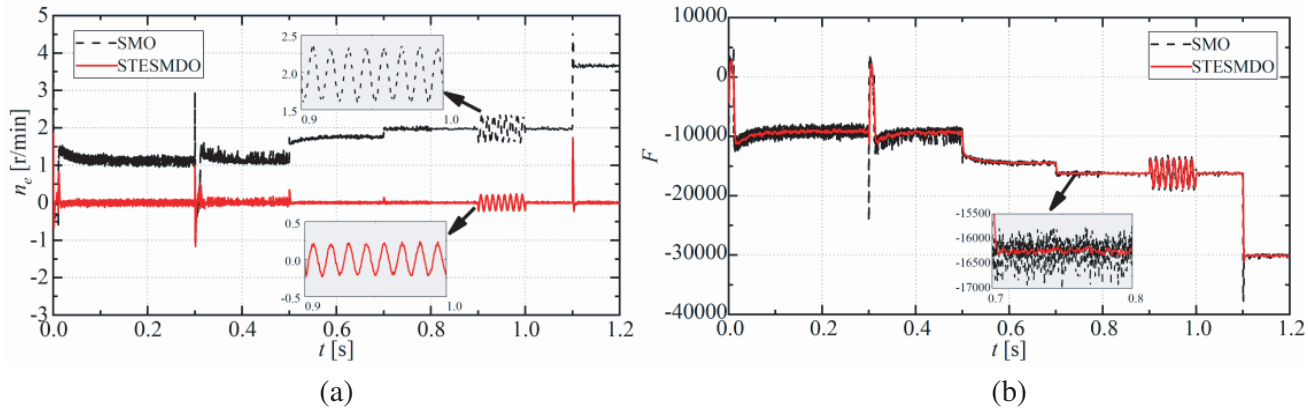

Figure 6. Simulation comparison results of SMO/STESMDO. (a) Speed tracking error e. (b) Unknown parts of the total perturbation F.

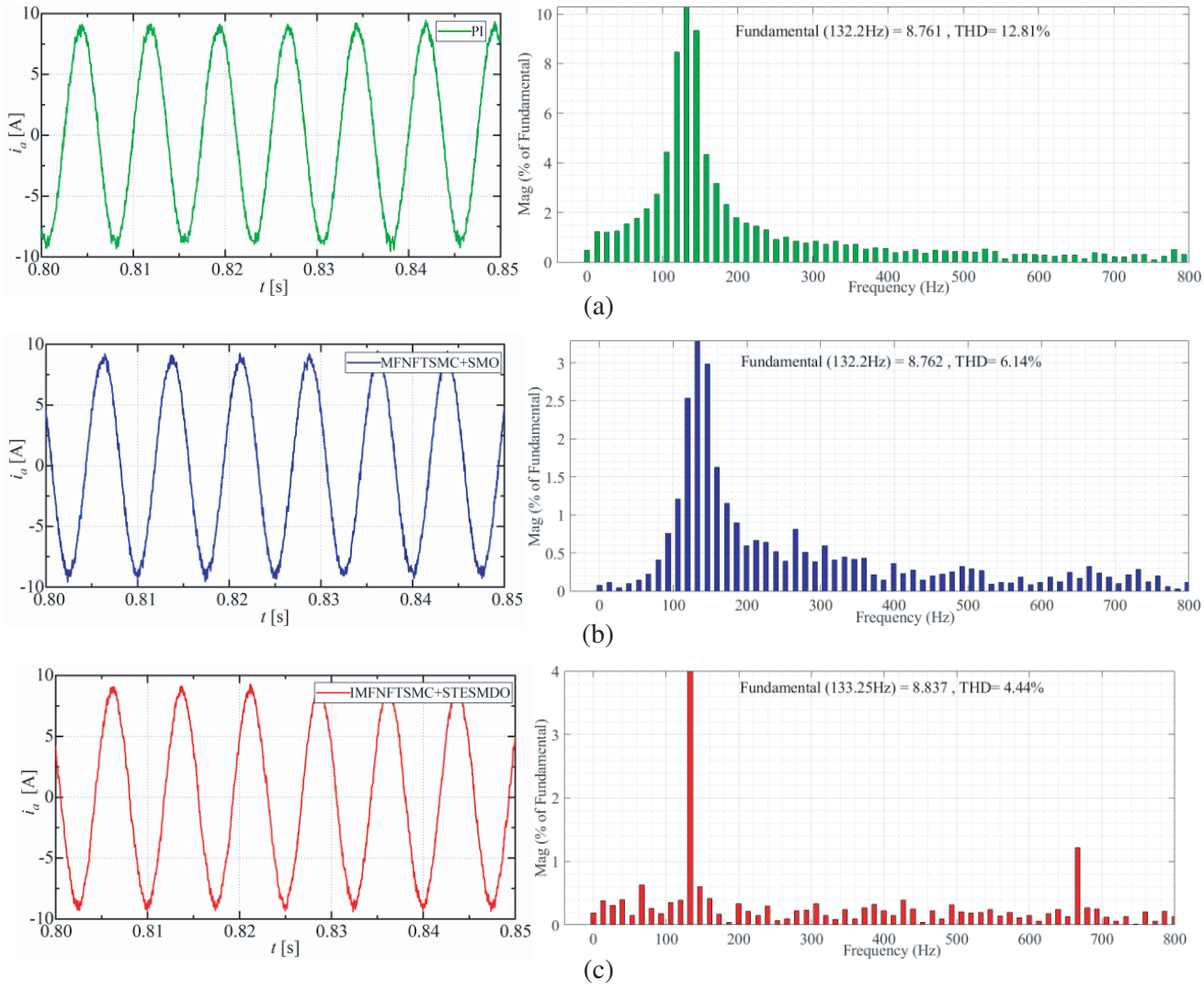

Figure 7. The THD analysis of A phase stator current. (a) PI. (b) MFNFTSMC. (c) IMFNFTSMC.

rate analysis (total harmonic distortion, THD) under the steady-state operation of the motor are given in Fig. 7. The PI phase current has more harmonic components because of parameters ingestion and time-varying disturbance, and its THD is 12.81%. In the MFNFTSMC algorithm, the THD is reduced to 6.14% due to the feedback of the SMO estimation of F, which suppresses certain harmonics, and thus provides better robustness. In the proposed IMFNFTSMC algorithm, the current THD is further weakened because of its NFTSM and second-order super-twisting combined with the designed controller and the design of STESMDO to F more accurate estimation feedback controller, so that the SPMSM system has a strong anti-disturbance capability, which can better ensure the safe and smooth operation of SPMSM under the parameter ingestion and time-varying disturbances, and therefore its THD is reduced to 4.44%.

4.2. Analysis of RT-Lab Experimental Results

To further verify the effectiveness of the method, hardware-in-the-loop simulation (HILS) experiment is conducted on the RT-Lab platform for the SPMSM. Fig. 8 is the RT-Lab experimental platform. Fig. 9 shows the experimental diagram of PI/MFNFTSMC/IMFNFTSMC, and the experimental conditions are set by the simulation requirements.

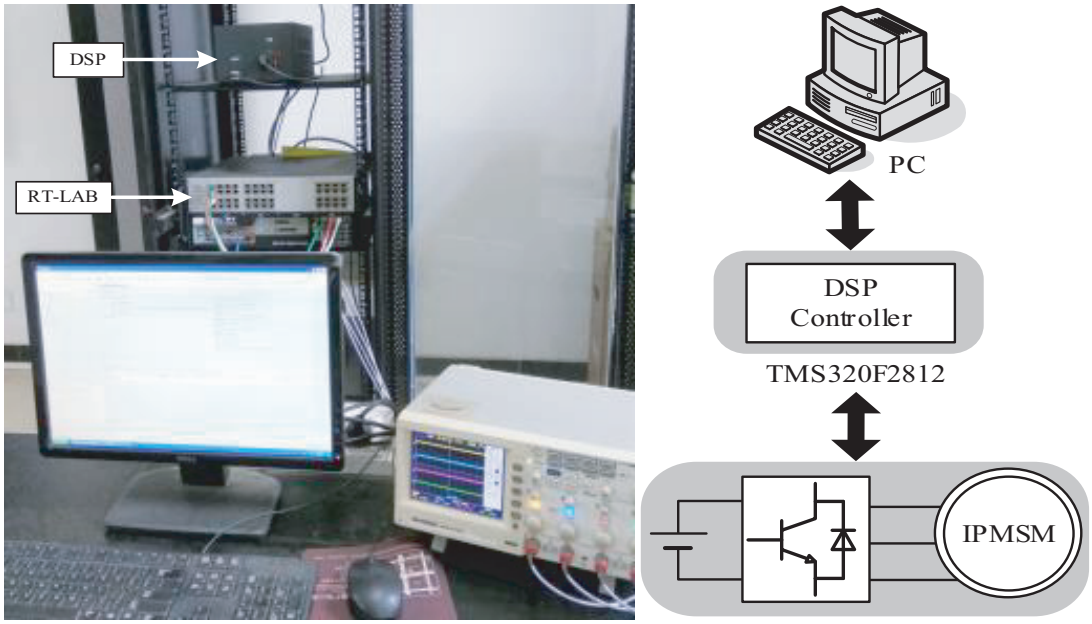

Figure 8. RT-LAB experimental platform.

From Fig. 8, RT-Lab (OP5600) is used to simulate the remaining components of the motor system such as interior permanent magnet synchronous motor (IPMSM) and inverter, with a real digital signal processing (DSP) controller of model TMS320F2812. The hardware-in-the-loop semi-physical system used in this paper adopts the structure of actual controller+virtual controlled object to model the controlled object of the system, and the real-time simulator runs the solved model to interact with the real controller through the processing of the input and output signals of the simulator by the interface box, thus forming a semi-physical real-time simulation system. This structure is mainly used in controller design, development, testing, and modeling research of controlled objects. The hardware-in-the-loop semi-physical simulation platform experiments can be used to obtain experimental results consistent with the actual motor. The control algorithm is mainly realized by modifying the algorithm in the Simulink environment, and then downloading it to the RT-Lab controller to ensure that the platform parameters and indicators are normal and start running. The feasibility of the control algorithm is verified by analyzing and studying the real-time waveforms fed back from the monitoring interface.

Figures 9(a), (b), and (c) show the full-condition experimental plots of PI, MFNFTSMC, and IMFNFTSMC, respectively. Fig. 10 shows the localized enlarged plots of PI, MFNFTSMC, and IMFNFTSMC. From Fig. 9 and Fig. 10, it can be seen that the simulation results of the three algorithms are the same as the RT-Lab experimental results. Under complex working conditions, the PI and MFNFTSMC have larger pulsations of d-q axis currents, larger steady-state errors in torque, and more significant overshoot in speed, which cannot accurately track the set value, while the proposed STESMDO-based IMFNFTSMC has smooth waveforms, small d-q axis currents and torque pulsation, and low current distortion rate. Therefore, the RT-Lab experiments further verify the feasibility of the proposed algorithm. When time-varying load disturbance occurs in the system at 0.9 s, PI controller has not yet reached the convergence and cannot satisfy the high performance of the system. When the time-varying perturbation has already entered into the next second, PI cannot satisfy the high performance of the system. The MFNFTSMC is able to carry out the stable tracking to a certain degree due to the role of the SMO. Table 3 shows the comprehensive performance comparison of the three methods.

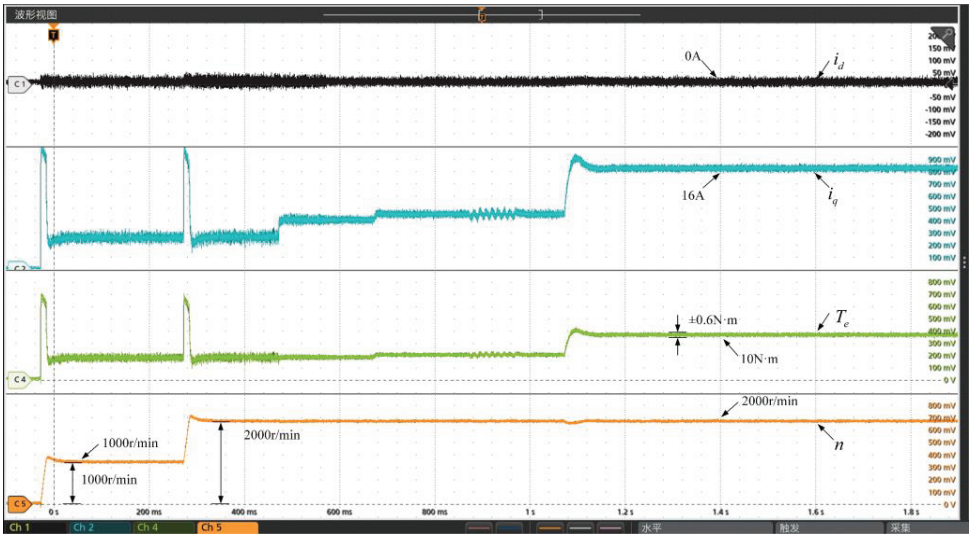

(a)

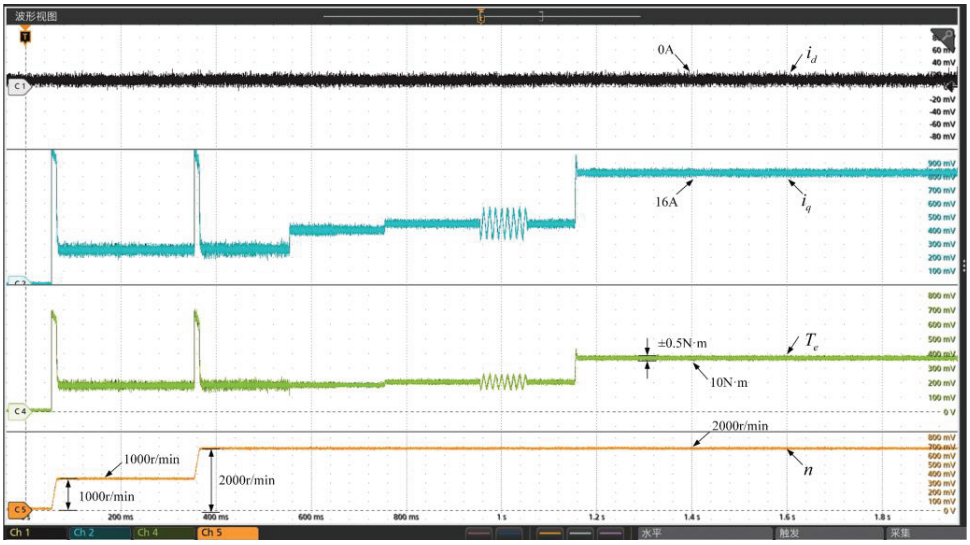

(b)

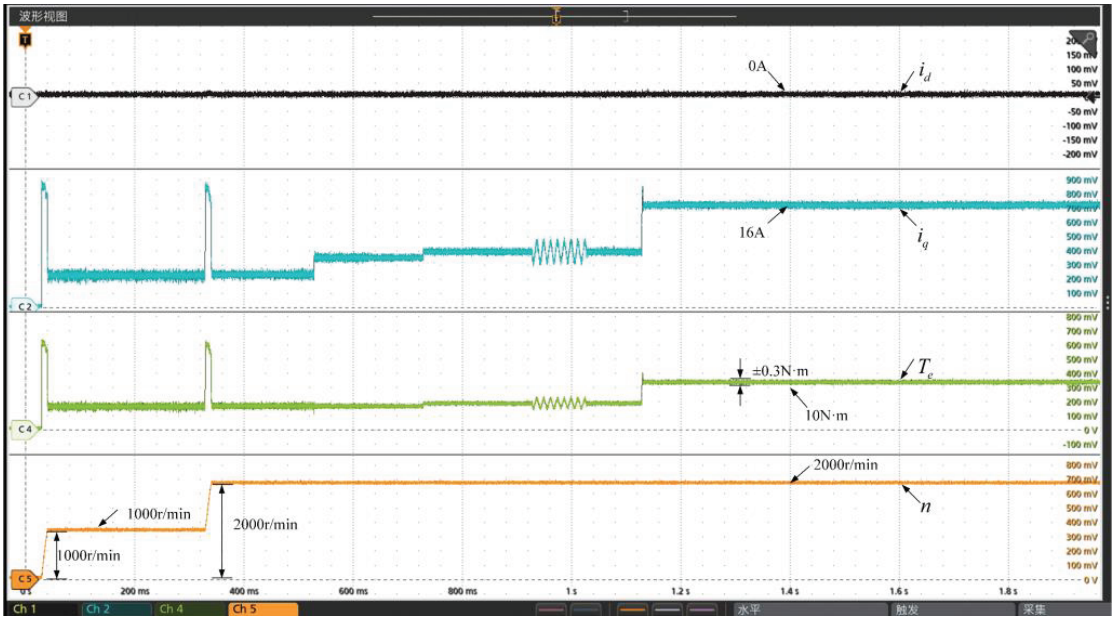

(c)

Figure 9. Comparison of experiment results. (a) PI. (b) MFNFTSMC. (c) IMFNFTSMC.

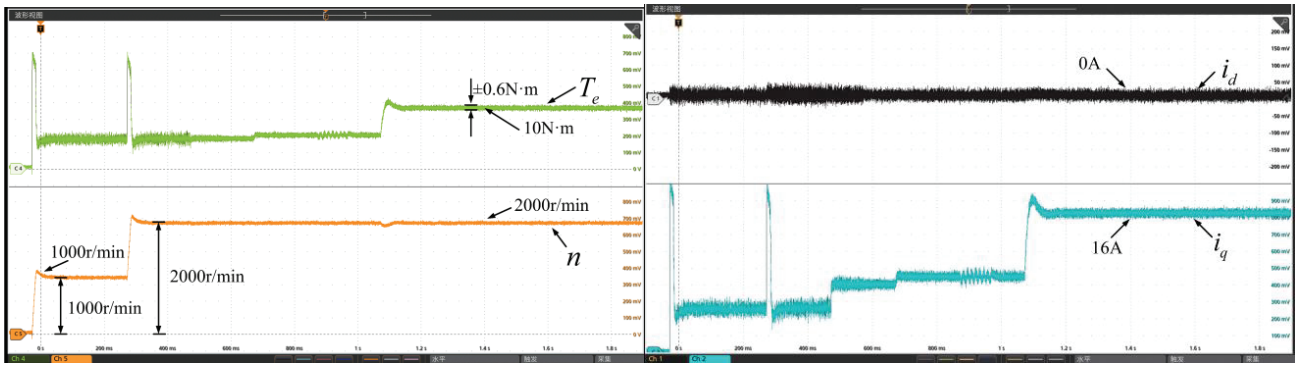

(a)

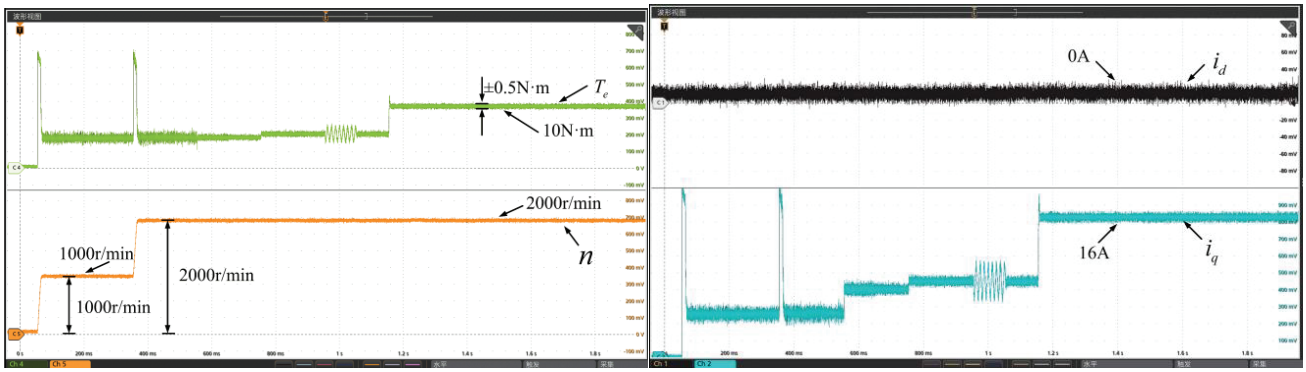

(b)

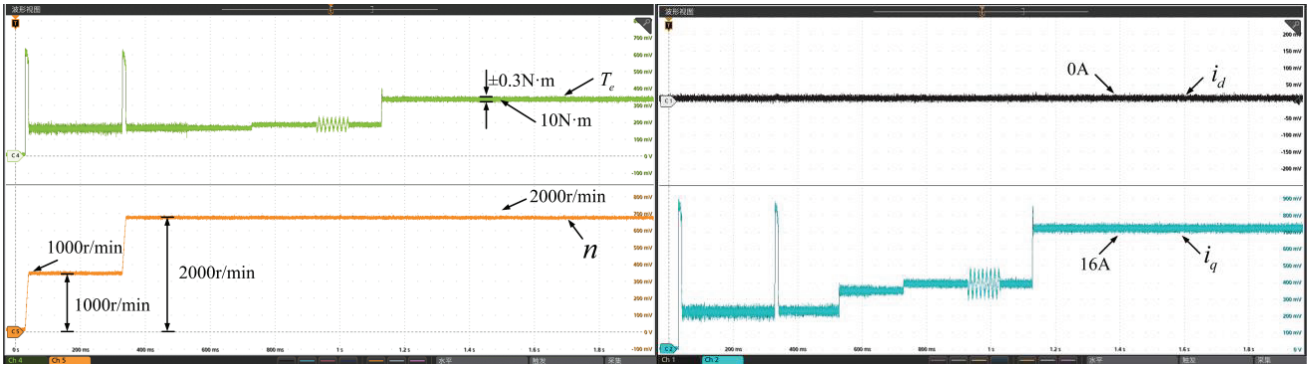

(c)

Figure 10. Comparison of experiment results of enlargement. (a) PI. (b) MFNFTSMC. (c) IMFNFTSMC.

Table 3. The comparison of comprehensive performance.

Performance indicators	PI	MFNFTSMC	IMFNFTSMC
Speed convergence time	0.05/0.06	0.03/0.02	0.01/0.01
Torque ripple	12.7%	10.3%	6.2%
$\bar{n}$ static difference	1.0/1.2	0.5/0.6	0.3/0.2
i_a THD	12.81%	6.14%	4.44%

5. CONCLUSION

The STESMDO based on IMFNFTSMC algorithm is proposed for the problems of SPMSM stability degradation caused by motor parameters ingestion and external time-varying disturbance. The correctness and superiority of the proposed method is verified through comparative analysis with conventional PI and MFNFTSM. The following conclusions are drawn: The designed new IMFNFTSM speed loop controller can speed up the system convergence. The designed STESMDO accurately estimates the unknown disturbance F of the system and feedbacks to the controller to improve the control accuracy and robustness of the system. The proposed algorithm is experimentally proven to be effective in reducing current and torque pulsations, improving speed control accuracy, and achieving fault-tolerant control of SPMSM under complex operating conditions.

ACKNOWLEDGMENT

This work was supported by the Natural Science Foundation of China (NSFC) under Grant 61473117, Grant 62173137, and Grant 2021YFF0501100, and in part by Postgraduate Scientific Research Innovation Project of Hunan Province under Grant CX20231107.

REFERENCES

1. Zhao, K., T. Yin, C. Zhang, et al., "Research on model-free sliding mode control of permanent magnet synchronous motor," *Journal of Electronic Measurement and Instrumentation*, Vol. 32, No. 4, 172–180, 2018.

2. Zhao, K., R. Zhou, A. Leng, et al., "Finite control set model-free fault-tolerant predictive control for permanent magnet synchronous motor," *Transactions of China Electrotechnical Society*, Vol. 36, No. 1, 27–38, 2021.
3. Zhao, K., W. Liu, Z. Liu, et al., "A model-free high-order Sliding mode control algorithm for permanent magnet synchronous motors," *Journal of Electrical Technology*, Vol. 38, No. 06, 1472–1485, 2023.
4. Liu, W., S. Chen, and H. Huang, "Adaptive nonsingular fast terminal sliding mode control for permanent magnet synchronous motor based on disturbance observer," *IEEE Access*, Vol. 7, 153791–153798, 2019.
5. Sun, B. Q., X. W. Ge, and Y. B. Sun, "Dynamical integral sliding mode control for permanent magnet ring torque motor," *Advanced Materials Research*, Vol. 383–390 (383–390), 799–804, 2011.
6. Tran, M.-D. and H.-J. Kang, "Nonsingular terminal sliding mode control of uncertain second-order nonlinear systems," *Mathematical Problems in Engineering*, Vol. 2015, No. 20, 2015.
7. Kang, E., J. He, and Y. Wang, "Design of nonsingular terminal sliding mode controller for permanent magnet synchronous motor," *Electric Machines and Control*, Vol. 25, No. 12, 58–64, 2021.
8. Tang, J., H. Zhou, Z. Zhang, et al., "A sensor-less control strategy for permanent magnet synchronous motor equipped with super-twisting sliding mode observer," *Journal of Detection and Control*, Vol. 45, No. 02, 115–121, 2023.
9. Chalanga, A., S. Kamal, and L. Fridman, "Implementation of super-twisting control: Super-twisting and higher order sliding-mode observer-based approaches," *IEEE Transactions on Industrial Electronics*, Vol. 63, No. 6, 3677–3685, 2016.
10. Li, Z. J., L. J. Wang, Y. N. Zhang, X. Y. Jia, et al., "Super-twisting second-order sliding mode APF current tracking control," *Journal of Electric Power Systems and Automation*, Vol. 32, No. 6, 36–42, 2020.
11. Swikir, A. and V. Utkin, "Chattering analysis of conventional and super-twisting sliding mode control algorithm," *2016 14th International Workshop on Variable Structure Systems*, 98–102, IEEE, Nanjing, 2016.
12. Mat, M., "Nonlinear control of autonomous underwater glider based on Super-Twisting Sliding Mode Control (STSMC)," *2017 7th IEEE International Conference on System Engineering and Technology*, 71–76, IEEE, Chengdu, 2017.
13. Huang, Z. F., J. P. Zhou, D. J. Mao, et al., "Passive super-twisting second-order sliding mode control strategy for MMC-UPQC under unbalanced grid voltage," *Control and Decision*, 1–10, June. 15, 2023.
14. Hou, Q. and S. Ding, "Finite-time extended state observer based super-twisting sliding mode controller for PMSM drives with inertia identification," *IEEE Transactions on Transportation Electrification*, Vol. 8, No. 2, 1918–1929, 2021.
15. Zhao, K., T. Yin, C. Zhang, J. He, et al., "Robust model-free nonsingular terminal sliding mode control for PMSM demagnetization fault," *IEEE Access*, Vol. 7, 15737–15748, 2019.
16. Zhao, K., W. Dai, R. Zhou, et al., "New modelless Sliding mode control of permanent magnet synchronous motor based on extended sliding mode disturbance observer," *Chinese Journal of Electrical Engineering*, Vol. 42, No. 06, 2375–2386, 2022.
17. Wang, Z., Y. Liao, C. Wei, et al., "Sliding mode guaranteed performance fault-tolerant control for the fast terminal of hypersonic aircraft," *Journal of Aeronautics*, 1–15, April 18, 2023.
18. Karamanakos, P. and T. Geyer, "Guidelines for the design of finite control set model predictive controllers," *IEEE Transactions on Power Electronics*, Vol. 35, No. 7, 7434–7450, 2019.
19. Huang, Y., R. Tang, M. Kuang, et al., "Improved modelless Sliding mode control of permanent magnet synchronous motor drive system based on fast approaching law," *Locomotive Electric Drive*, Vol. 03, 148–155, 2022.
20. Huang, Z., J. Zhou, D. Mao, et al., "Passive super spiral second-order Sliding mode control strategy of MMC-UPQC under unbalanced grid voltage," *Control and Decision-making*, 1–10, April 18, 2023.